Available online at www.sciencedirect.com
ScienceDirect
Journal of Power Sources 159 (2006) 734–741
JOURNAL OF POWER SOURCES
www.elsevier.com/locate/jpowsour

Characterization of sol–gel-derived NiO_x xerogels as supercapacitors

Jie Cheng *, Gao-Ping Cao, Yu-Sheng Yang

Research Institute of Chemical Defense, Beijing 100083, China

Received 27 March 2005; received in revised form 27 July 2005; accepted 29 July 2005
Available online 18 January 2006

Abstract

NiO_x xerogels were formed by the sol–gel method followed by heat-treatment under ambient pressure. The structure and properties of these materials were characterized by using X-ray diffraction, XPS, TEM, TGA–DTA and N_2 (77 K) adsorption. Electrodes with the xerogels were activated by cyclic voltammetry (CV) and their capacitive performance was evaluated by CV and galvanostatic technique in 7 M KOH solutions. A maximum specific capacitance of 696 F g^{-1} was obtained by constant current discharge with a current density of 2.0 mA cm^{-2} for the NiO_x xerogels heat-treated at 250 °C. The results of in situ XRD of the NiO_x xerogels after the charge/discharge recycling test showed that the NiO_x xerogels might exhibit faradaic pseudocapacitance by surface redox from $Ni(OH)_2$ to NiOOH. The high performance obtained indicates that these materials are promising electrode materials for supercapacitors.

Keywords: Supercapacitor; NiO_x xerogels; Cyclic voltammetry; Galvanostatic technique

1. Introduction

Supercapacitors have attracted considerable attention in recent years for their use in high power applications [1,2]. Most commercial supercapacitors store energy in electric double layer. The capacitance of an electric double layer is typically in the range of 10–40 μF cm^{-2} [3] and the voltage is limited by the electrochemical stability of the electrolyte. Faradaic pseudocapacitance can enhance the energy storage of the supercapacitors [3], transition metal oxides, such as Co_2O_3 [4], RuO_2 [5–7] and V_2O_5 [8], exhibit faradic pseudocapacitance.

Recently, NiO materials have received much attention due to the low cost of raw materials, low toxicity, and their environmentally friendly character. Studies of Liu and Anderson [9] and Srinivasan and Weidner [10] have shown that NiO materials formed by heating electro chemically derived $Ni(OH)_2$ are promising electrode materials for supercapacitors. The highest specific capacitance of these materials is 278 F g^{-1}.

Since the electric double-layer capacitance and the pseudocapacitance are interfacial phenomena, the materials for supercapacitors should possess a high specific surface area to enhance the charge-storage capability. The sol–gel method can give the materials superior properties, including (1) high specific surface area; (2) stabilization of nanoscale matter to coalescence or agglomeration; (3) rapid mass transfer through the continuous volume of mesopores. Considering these aspects, we prepared NiO_x xerogels using the sol–gel method followed by heat-treatment under ambient pressure. The resulting NiO_x xerogels behaved as supercapacitors with a maximum specific capacitance of 696 F g^{-1} under constant current discharge with a current density of 2.0 mA cm^{-2} in 7 M KOH solutions. At the same time, in situ XRD spectra showed that after the charge/discharge cycle, there was $Ni(OH)_2$ in the NiO_x xerogels prepared by heating at high temperature, indicating that the NiO_x xerogels might exhibit faradaic pseudocapacitance by a surface redox from $Ni(OH)_2$ to NiOOH.

2. Experimental

$NiSO_4{\cdot}6H_2O$, KOH, $Na_3C_6H_5O_7{\cdot}2H_2O$ and $NaOOCCH_3$ of analytical grade purity were used. In order to achieve $Ni(OH)_2$ gels, a simple process was developed, as the follows. An aqueous solution consisting of 30 g L^{-1} $NiSO_4{\cdot}6H_2O$, 13 g L^{-1} $Na_3C_6H_5O_7{\cdot}2H_2O$ and 5 g L^{-1} $NaOOCCH_3$ was kept stirred at a constant temperature of 80 °C under ambient pressure. A 3 M aqueous solution of KOH was dropwise added into the

* Corresponding author. Tel.: +86 10 66705840; fax: +86 10 66748574.
E-mail addresses: chengjie_chj@sohu.com, chengjie.chj@163.com (J. Cheng).

0378-7753/$ – see front matter © 2005 Elsevier B.V. All rights reserved.
doi:10.1016/j.jpowsour.2005.07.095

above solution until the pH of the solution reached 12. The resulting suspension was centrifuged and rinsed repeatedly with distilled water and ethanol. $Ni(OH)_2$ gels were then obtained. The gels were heated to 80 °C and held there until dried enough. Temperature-programmed calcination in air was used in the final preparation step to achieve the NiO_x xerogels. The dried gels were heated at a rate of 5 °C min^{-1} to the calcinations temperature (which varied from 110 to 450 °C), held there for 1 h, and then allowed to cool naturally. The BET specific surface area and pore volume of the xerogels were determined by means of nitrogen gas adsorption at 77 K with micrometrics ASAP 2010. The pore size distribution of $Ni(OH)_2$ xerogels was calculated according to BJH method by using the desorption branch of the isotherm. A Rigaku D/MAX-RB diffractometer using Cu Kα radiation was used to obtain the crystalline information of the samples. ANETZSCH STA449C Jupiter® thermogravimetric analyzer was used to determine the weight loss of the dried gels during calcination in air at a heating rate of 5 °C min^{-1}. Elemental composition analysis of the samples was carried out by X-ray photoelectron spectroscopy (XPS) by using a PHI 5300 X-ray Photoetectron Spectrometer. The XPS analysis was performed with a monochromatic Mg Kα source operating at 250 W with a pass energy of 20 eV and a step of 0.1 eV transmission electron microscopy (TEM) was used to characterize the microstructure of the samples.

All electrochemical measurements were carried out using a Solartron 1280Z workstation in a three-electrode configuration assembly consisting of active carbon as the counter electrode, NiO_x xerogels as the working electrode and Hg/HgO (7 M KOH aqueous electrolyte) as the reference electrode. The working electrodes were made as follows. A slurry of NiO_x xerogels was formed with a weight ratio of NiO_x xerogels: carbonblack: CMC = 94:5:1. The slurry was coated onto single side of a piece of nickel foam sheet. Another piece of nickel foam sheet was put onto the coated side to sandwich the NiO_x materials and then the sandwiched sheets were dried and pressed to form a working electrode. The working electrode contained about 30 mg NiO_x xerogels on an apparent area of 1.0 cm^2. An activation process was carried out in a potential window from 0.25 to 0.65 V versus Hg/HgO at a scan rate of 1 mV s^{-1}. The electrochemical performance was evaluated by using the cyclic voltammetry (CV) and galvanostatic technique. CV was conducted in a potential range between 0.20 and 0.60 V versus Hg/HgO at a scan rate of 1 mV s^{-1}. A constant current discharge test was carried out at different currents after a 10-min potentiostatic process at 0.60 V versus Hg/HgO.

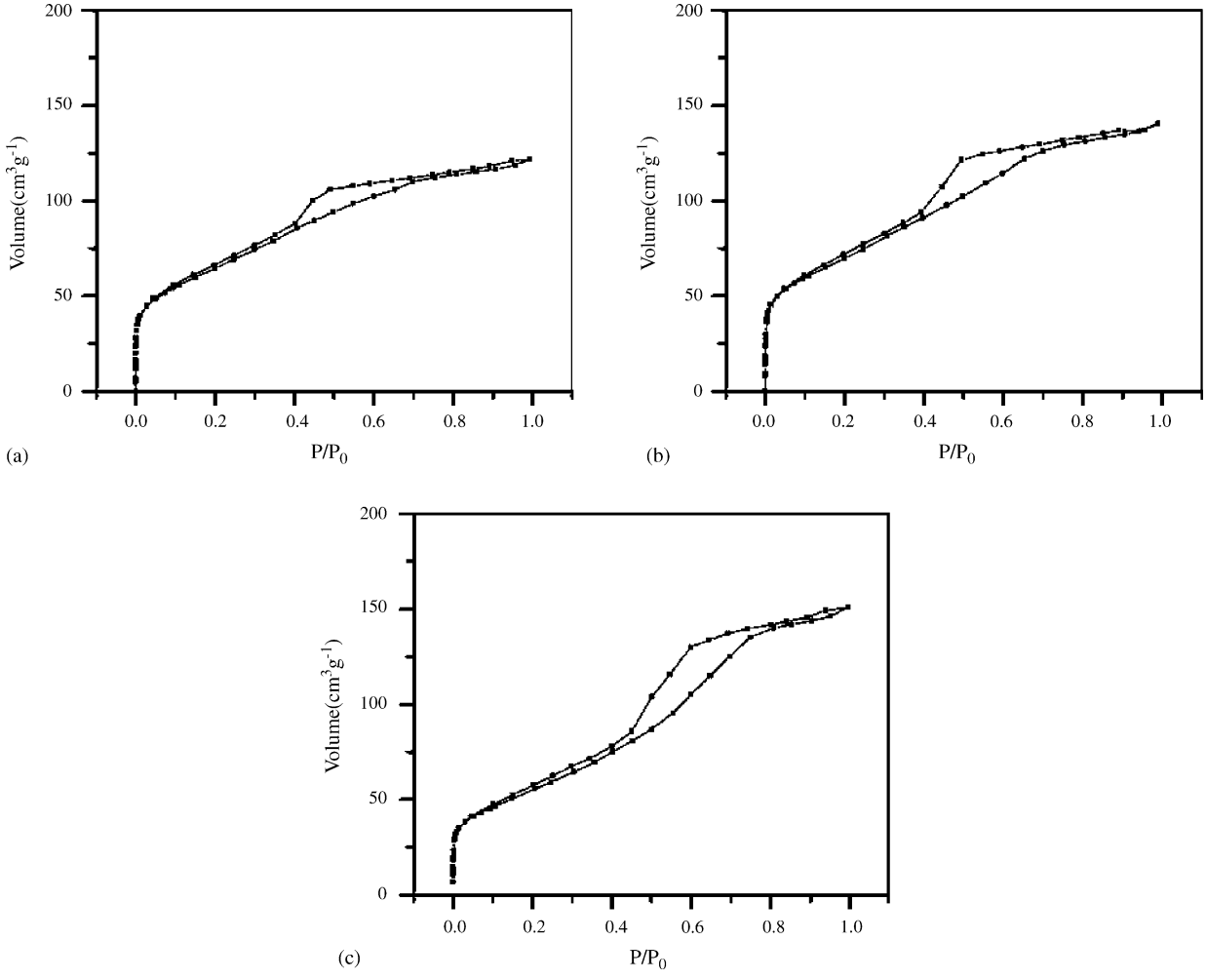

Fig. 1. Nitrogen absorption/desorption isotherm (77 K) of the NiO_x xerogels heat-treated at different temperatures: (a) 110 °C, (b) 250 °C, and (c) 450 °C.

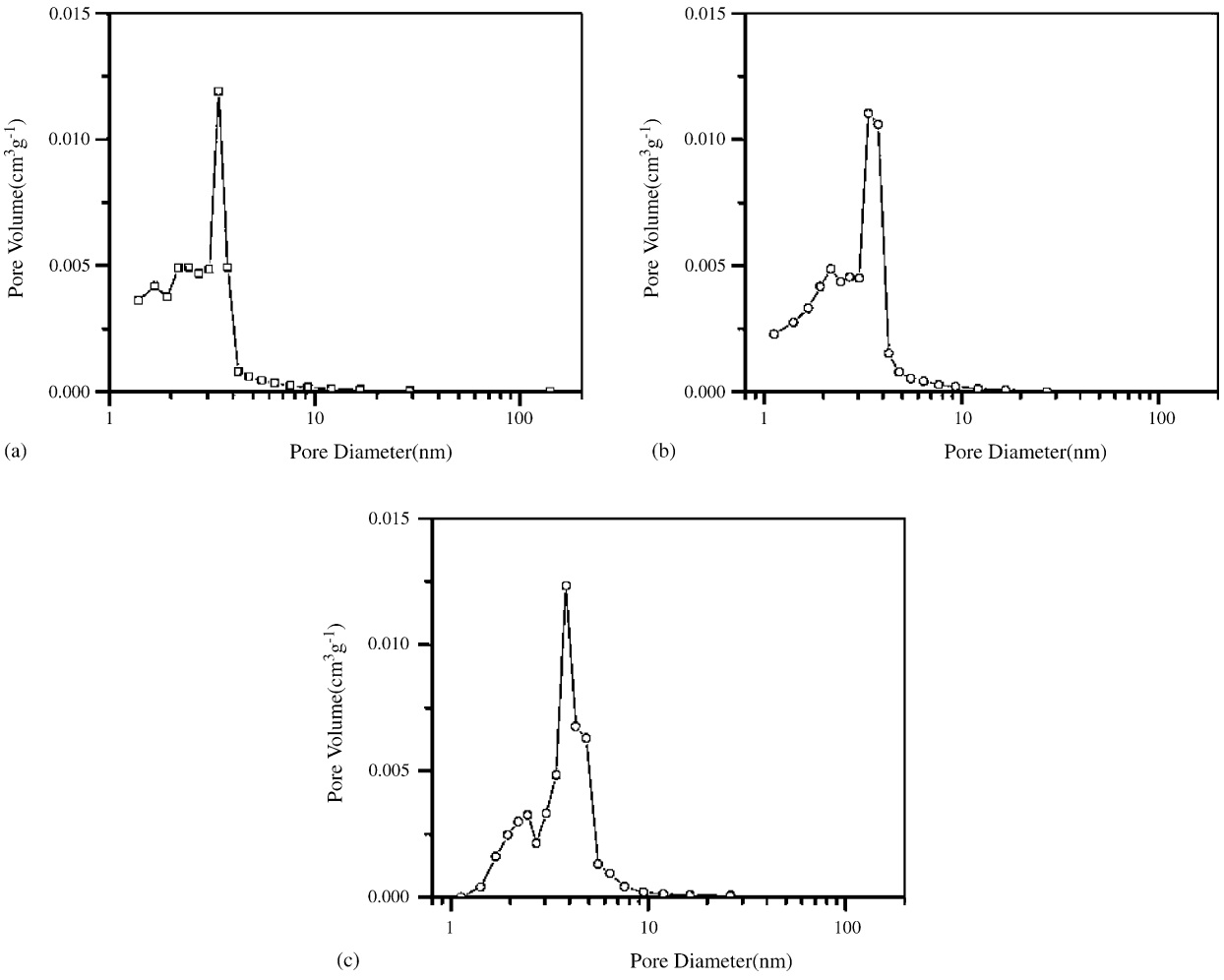

Fig. 2. Pore size distribution of the NiO_x xerogels calculated by BJH method by using the desorption branch of the isotherm: (a) 110 °C, (b) 250 °C, and (c) 450 °C.

3. Results and discussion

The typical nitrogen gas absorption/desorption isotherms of the NiO_x xerogels are shown in Fig. 1. All the samples displayed an isotherm of type IV and a hysteresis loop of type H_2 according to the IUPAC classification. The hysteresis loop is indicative of mesoporosity.

By using the desorption branch of the isotherm, the pore size distribution of the NiO_x xerogels calculated by BJH method were derived as shown in Fig. 2. One can see that the pore size distribution is mainly in the region of 1–10 nm and the mesopore structure is almost changeless as the calcination temperature increases. This indicates that the NiO_x xerogels obtained have a stable and well-developed mesopore structure.

The effect of thermal treatment on the specific surface area and pore volume of the NiO_x xerogels is shown in Fig. 3. The specific surface area initially decreased with an increase in temperature from 200 to 300 °C and reached a maximum of 285 $m^2\ g^{-1}$ at 300 °C and then decreased with a further increase in temperature. The pore volume increased with an increase in temperature from 110 to 280 °C, and kept constant in the range between 280 and 400 °C, and then decreased slightly to 450 °C. It is the variation of the micropores of the NiO_x xerogels that has caused a surface area shift, while the mesopore structure remains almost stable relative to the pore size distribution of the NiO_x xerogels.

The effect of the calcination temperature on the crystalline structure of the NiO_x xerogels is shown in Fig. 4 in terms of the

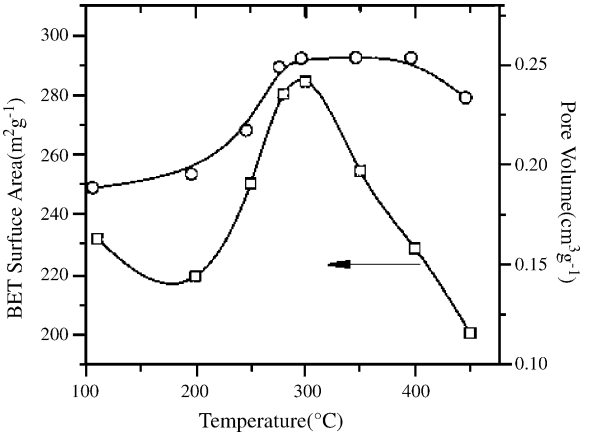

Fig. 3. Effect of the calcination temperature on both the specific surface area and pore volume of the NiO_x xerogels.

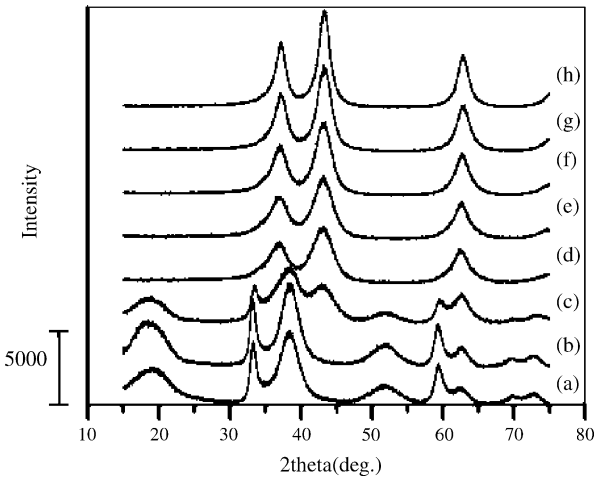

Fig. 4. XRD of the NiO_x xerogels heated at different temperatures: (a) 110 °C, (b) 200 °C, (c) 250 °C, (d) 280 °C, (e) 300 °C, (f) 350 °C, (g) 400 °C, and (h) 450 °C.

XRD patterns. Below 200 °C, all the distinct diffraction peaks of the NiO_x xerogels consist with those of β-$Ni(OH)_2$ (such as JCPDF card 74-2075). As the temperature increased from 250 to 280 °C, distinct diffraction peaks of NiO (such as JCPDF card 47-1049) were observed. Above 280 °C, the XRD patterns exhibited only the characteristic peaks of NiO, and the intensities of the peaks increased as the temperature increased, indicating that more crystallization was taking place.

Thermogravimetric and differential thermal analyses (TG–DTA) were carried out on the dried $Ni(OH)_2$ gels to investigate their thermal behavior. The corresponding patterns are illustrated in Fig. 5 with commercial $Ni(OH)_2$ as a reference. The weight loss of the dried $Ni(OH)_2$ gels occurred in three stages: (1) an initial loss of about 7.9% up to 200 °C, corresponding to removal of the water of hydration and absorbed water, (2) a rapid loss of about 12.0% between 250 and 320 °C, corresponding to removal of the water due to the decomposition of the $Ni(OH)_2$ to NiO_x, and (3) an additional rapid loss of about 4.3% between 390 and 420 °C.

According to the decomposition reaction equation of $Ni(OH)_2$:

$$Ni(OH)_2 \xrightarrow{\Delta} NiO + H_2O \uparrow \quad (1)$$

the total weight loss is about 19.4%, close to the weight loss of the commercial $Ni(OH)_2$ which is about 17.8%. Both the weight loss of the dried $Ni(OH)_2$ gels in the latter two stages are about 16.3%, close to the weight loss of the commercial $Ni(OH)_2$. We speculate that the decomposition of the dried $Ni(OH)_2$ gels might include two steps, i.e., decomposition of the crystalline β-$Ni(OH)_2$ occurs between 250 and 320 °C, and decomposition of the amorphous $Ni(OH)_2$ occurs between 390 and 420 °C.

XPS measurements were performed for a better understanding of the previous results. Fig. 6 shows the XPS data of the NiO_x xerogels for full scan and Ni 2p. For a charge correction on the samples, the peak of the C 1s line (284.6 eV) [11] from adventitious hydrocarbon was used as a reference. As shown in Fig. 6(a), only Ni and O were observed according to the full scan results of all the samples. In Fig. 6(b), there was only one dominant peak at 855.7 eV for the Ni 2p spectra of the NiO_x xerogels heated at 200 °C, but there were two dominant peaks at 854.3 and 855.7 eV for the Ni 2p spectra of the NiO_x xerogels heated above 200 °C. The dominant Ni $2p_{3/2}$ peaks of 854.3 and 855.7 eV are consistent with the Ni $2p_{3/2}$ peaks for NiO and $Ni(OH)_2$ [11], respectively.

An analysis of the O ls peak can give useful information regarding the state of oxygen bonding of the samples. Fig. 7(a)–(d) shows the XPS spectra of O ls. There was only one binding energy peak at 531.3 eV for the O ls spectra of the NiO_x xerogels heated at 200 °C shown in Fig. 7(a), but there were two binding energy peaks at 529.5 and 531.3 eV respectively for the O ls spectra of the NiO_x xerogels heated above 200 °C as shown in Fig. 7(b)–(d). The dominant O ls peaks of 529.5 and 531.3 eV are consistent with the O ls peak of NiO and $Ni(OH)_2$ or Ni_2O_3 [11], respectively. The peak area of 529.5 eV increased with an increase in temperature from 250 to 450 °C while the peak area of 531.3 eV decreased, indicating that the x in NiO_x decreased. The XPS study showed that the nickel oxides

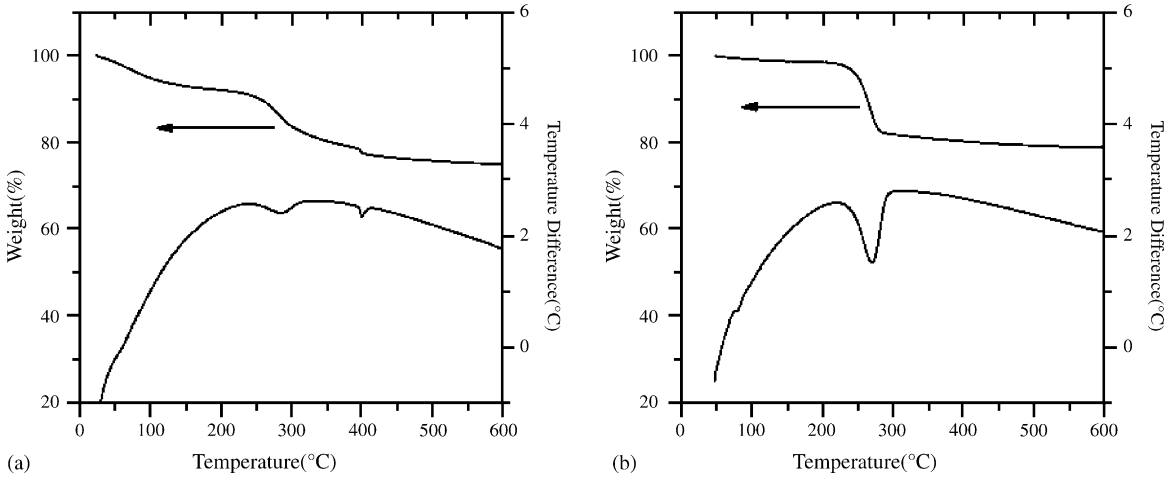

Fig. 5. TG A and DTA plots for (a) dried $Ni(OH)_2$ gels and (b) commercial $Ni(OH)_2$.

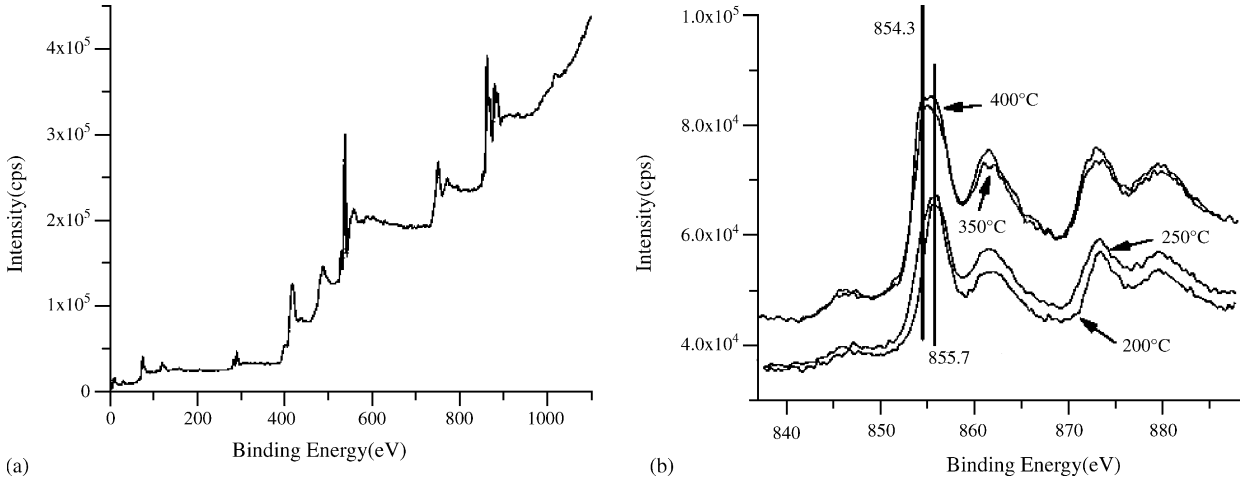

Fig. 6. The XP spectra of the NiO_x xerogels: (a) full scan and (b) Ni 2p spectra.

are nonstoichiometric [12], thus the nickel oxide in this paper could be denoted as NiO_x. The element ratio calculated from XPS data was listed in Table 1 (H excluded).

Fig. 8 represents the TEM micrograph of the NiO_x xerogels heated at 110 °C. The TEM image shows many micro-stripes of nanocrystals with a size about 10 nm, indicating that the NiO_x xerogels consist of nanocrystalline β-$Ni(OH)_2$, amorphous materials and many nanopores.

The activation of the NiO_x xerogels calcined at 110 °C by using CV is shown in Fig. 9. The CV current of the electrodes was found to increase gradually with charge–discharge recycle number, indicating that there was an activating process

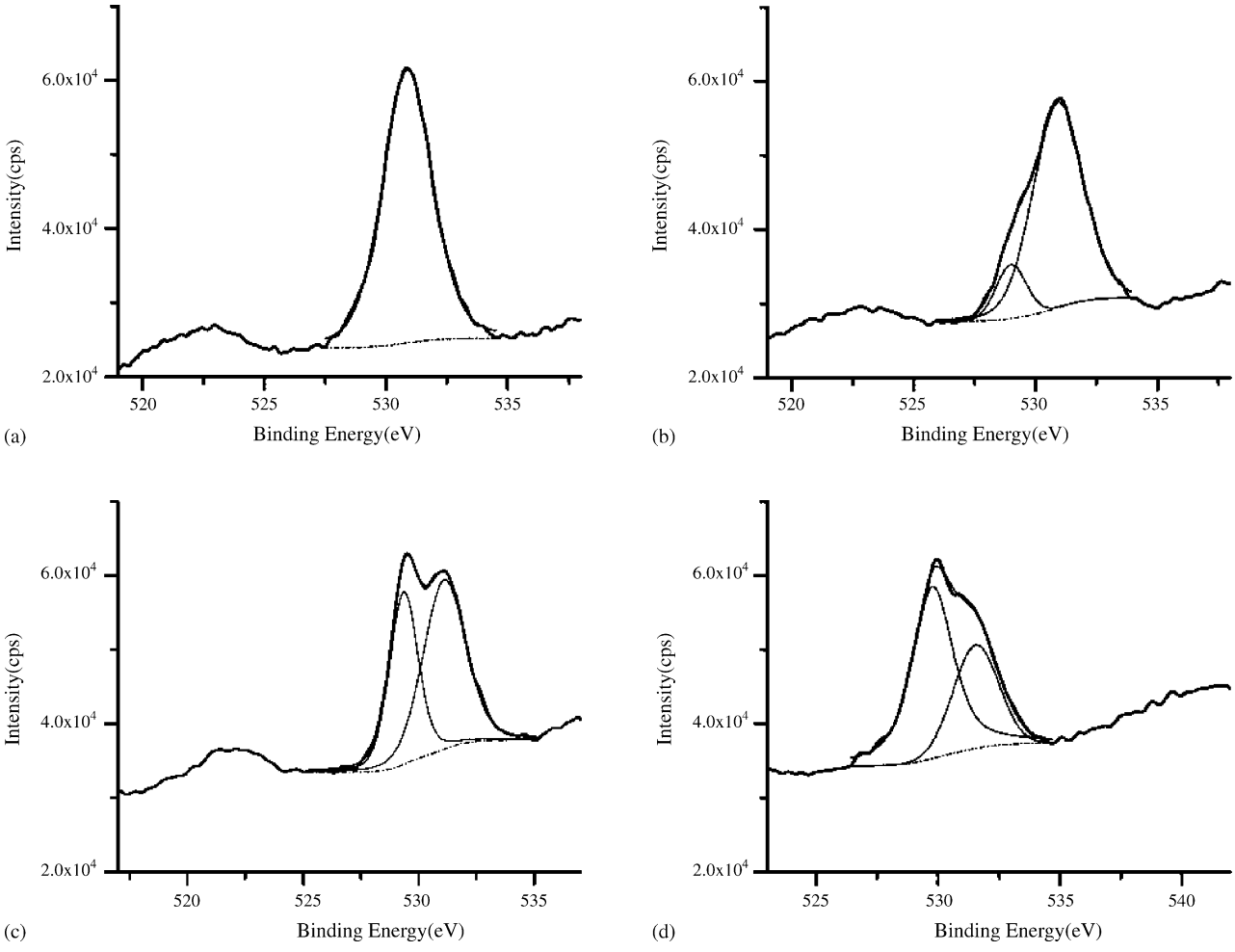

Fig. 7. XP spectra of the O ls for the samples: (a) 200 °C, (b) 250 °C, (c) 350 °C, and (d) 450 °C.

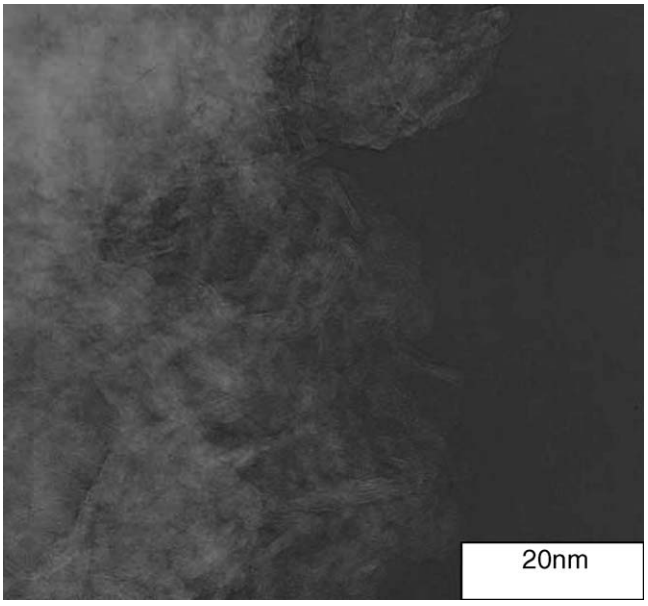

Fig. 8. TEM micrographs of the NiO_x xerogels calcined at 110 °C.

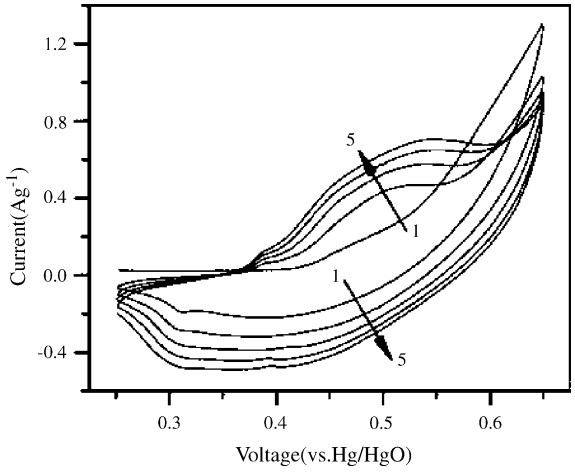

Fig. 9. Activation of the NiO_x xerogels cabined at 110 °C by using cyclic voltammetry at 1 mV s^{-1} in 7 M KOH (first five cycles).

Table 1
Element ratio of the NO_x xerogels heated from 110 to 450 °C (from XPS data, H excluded)

Sample (°C)	x in NiO_x
110	2.32
200	2.06
250	1.50
280	1.36
300	1.19
350	1.18
400	1.15
450	1.08

just like the $Ni(OH)_2$ electrodes in MH/Ni and Cd/Ni batteries. After 10 cycles the charge capacity tended to reach stability.

After activation, galvanostatic technique and CV were used to analyze the electrochemical properties of the NiO_x xerogels. Constant current discharge profiles of the NiO_x xerogels are shown in Fig. 10, where the charge process was measured as a potentiostatic process for 10 min at 0.60 V versus Hg/HgO. The corresponding specific capacitances were calculated from

$$C = \frac{I\Delta t}{m\Delta V} \quad (2)$$

where I is the discharge current, Δt the total discharge time, m the mass of the NiO_x xerogels, ΔV the potential drop during discharge, and C is the specific capacitance. The results are displayed in Table 2. The NiO_x xerogels calcined at 250 °C exhibited the highest specific capacitance of 696 F g^{-1} with a discharge current density of 2.0 mA cm^{-2}. This indicated that the capacitance of the NiO_x xerogels has been enhanced. The resulting patterns of the CVs are shown in Fig. 11. The potential was scanned between 0.20 and 0.60 V versus Hg/HgO at a scan rate of 1 mV s^{-1} in both directions and the current response was measured. All the curves exhibited almost the same shape and there were no obvious peaks, indicating that these electrodes exhibited perfect pseudocapacitance. These curves also

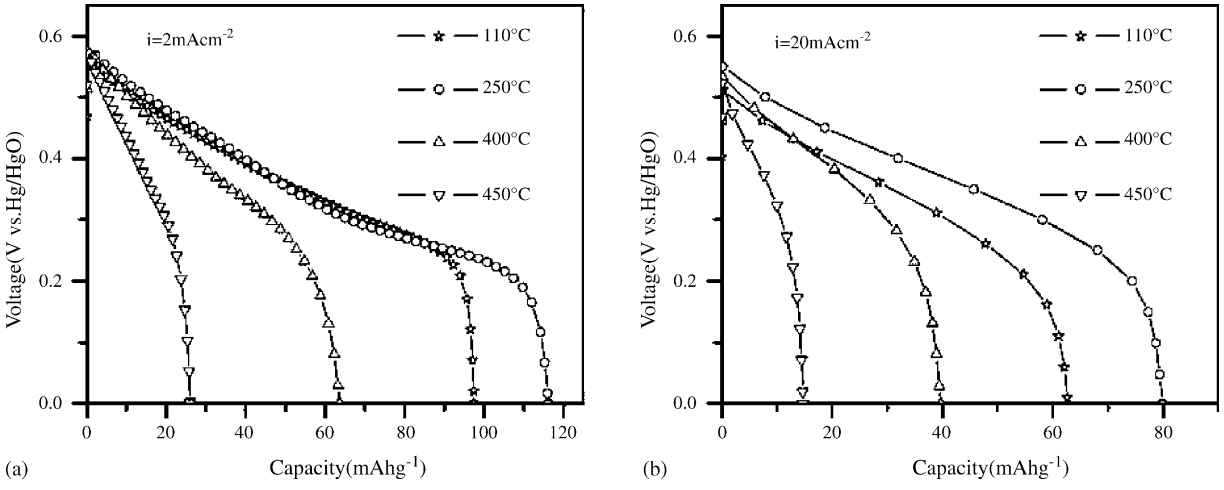

Fig. 10. The discharge behavior of the NiO_x xerogels (charging at 0.6 V vs. Hg/HgO for 10 min): (a, left) $i = 2$ mA cm^{-2} and (b, right) $i = 20$ mA cm^{-2}.

Table 2
Effect of the calcination temperature on the specific capacitance calculated from constant current discharge curves (charging at 0.6 V vs. Hg/HgO for 10 min)

Heating temperature (°C)	Specific capacitance F g^{-1} (0.60–0.00 V vs. Hg/HgO)		
	2 mA cm^{-2}	10 mA cm^{-2}	20 mA cm^{-2}
110	592	419	377
200	636	469	404
250	696	521	479
280	586	420	373
300	546	383	340
350	494	302	269
400	382	270	235
450	157	106	88.8

exhibited similar trends with those shown in Fig. 10; thus, these results were consistent with those obtained from galvanostatic techniques.

In recent studies of nickel oxide as a supercapacitor material [9,13], the electrochemical redox reaction of nickel oxide in alkaline solution could be expressed as below:

$$NiO + OH^- \Leftrightarrow NiOOH + e^- \quad (3)$$

According to the study of Kwang-Bum Kim and Kwang-Wan Kim [12], the electrochemical redox reaction of the NiO_x is not a simple adsorption/desorption reaction of OH^- ions, but rather is a two-step process. During the initial stage of oxidation, H^+ ions are released from the oxide surface to form H_2O with OH^- in the solution, followed by adsorption of OH^- ions in the solution onto the oxide surface during the latter stage of the oxidation. The reverse occurs during reduction.

In the present work, high specific capacitance was obtained. But at higher temperatures, such as 400–450 °C, the specific capacitance of the NiO_x xerogels decreased. In other words, the capacitance of the NiO_x xerogels slightly increased while the x in NiO_x decreased with a temperature increase from 100 to 250 °C. It reached a maximum of 696 F g^{-1} at 250 °C and sharply decreased as the x in NiO_x further decreased. We speculate that there might be another mechanism for charge storage. In order to get a better understanding of the nature of the charge-storage mechanism of the NiO_x xerogels, in situ XRD was used to observe the crystalline structure of the NiO_x xerogels after the charge/discharge test. The resulting patterns are shown in Fig. 12. After the charge/discharge recycling test, the distinct diffraction peaks of β-Ni(OH)$_2$ were observed in the spectra of the NiO_x xerogels heat-treated at temperatures from 280 to 400 °C. This indicated that the process might be expressed as (4):

$$NiO + H_2O \Rightarrow Ni(OH)_2 \quad (4)$$

or

$$NiO + OH^- \Rightarrow NiOOH + e^-,$$
$$NiOOH + H_2O + e^- \Rightarrow Ni(OH)_2 + OH^- \quad (5)$$

Since the specific capacitance of the NiO_x xerogels is larger when x in NiO_x is larger, the reversible pseudocapacitance redox reaction might be expressed as (6):

$$NiOOH + H_2O + e^- \Leftrightarrow Ni(OH)_2 + OH^- \quad (6)$$

In another words, a part of NiO in the NiO_x xerogels might store charge according to a process as (3), but another part of the NiO would transform to Ni(OH)$_2$ as shown (4) or (5), i.e., the Ni(OH)$_2$ might also store charge on the oxide surface.

At higher calcination temperatures, such as above 400 °C, the process of (4) or (5) was partially cut short because defective sites decreased as a result of crystallization. So the specific capacitance of the NiO_x xerogels decreased sharply as calcination temperature increased in the range from 400 to 450 °C.

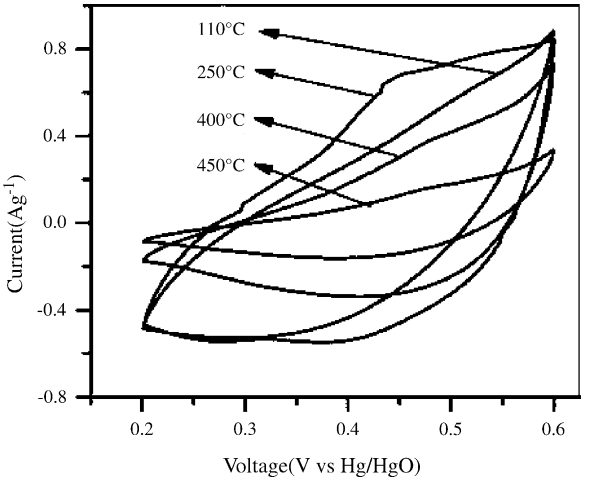

Fig. 11. Steady CV curves of the NiO_x xerogels at 1 mV s^{-1} in 7 M KOH.

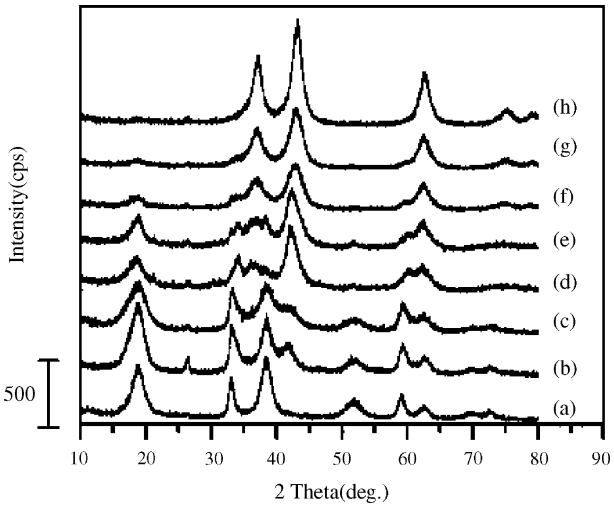

Fig. 12. XRD patterns of the NiO_x xerogels heated at different temperatures (after charge/discharge): (a) 110 °C, (b) 200 °C, (c) 250 °C, (d) 280 °C, (e) 300 °C, (f) 350 °C, (g) 400 °C, and (h) 450 °C.

4. Conclusions

NiO_x xerogels were formed by the sol–gel method at 80 °C and ambient pressure followed by heat-treatment in air. The NiO_x xerogels exhibited both high surface area and stable mesopore structure. The TGA–DTA study showed that

the decomposition of the dried $Ni(OH)_2$ gels might contain two parts, i.e., the decomposition of the crystal form occurs between 250 and 320 °C and the decomposition of the amorphous form occurs between 390 and 420 °C. At the calcination temperatures of 110–200 °C the crystalline structure of the NiO_x xerogels was β-$Ni(OH)_2$. However, crystalline NiO arose and increased with an increase in temperature from 250 to 450 °C.

Cyclic voltammetry study showed that the NiO_x xerogels have an activating process. The specific capacitance of the NiO_x xerogels initially increased with an increase of calcination temperature from 110 to 250 °C, and it reached a maximum of 696 F g^{-1} at 250 °C but decreased as the temperature continuingly increased. The high performance obtained indicates that the $Ni(OH)_2$ xerogels are promising electrode materials for supercapacitors.

In situ XRD was used to observe the crystalline structure of the NiO_x xerogels after the recycling test. The results showed that the distinct diffraction peaks of β-$Ni(OH)_2$ appeared in the spectra of the NiO_x xerogels heat-treated at temperatures from 280 to 400 °C. This indicated that $Ni(OH)_2$ might also store charge on the oxide surface, i.e., the NiO_x xerogels might exhibit faradaic pseudocapacitance by surface redox from $Ni(OH)_2$ to NiOOH.

Acknowledgement

Financial support from National 863 Program is gratefully acknowledged.

References

[1] B.E. Conway, Transition from 'supercapacitor' to 'battery' behavior in electrochemical energy storage, J. Electrochem. Soc. 138 (6) (1991) 1539–1548.
[2] E. Faggioli, P. Rena, V. Danel, X. Andrieu, R. Mallant, H. Kahlen, Supercapacitors for the energy management of electric vehicles, J. Power Sources 84 (2) (1999) 261–269.
[3] B.E. Conway, Electrochemical Supercapacitore Scientific Fundamentals and Technological Applications, Plenum Press, 1999.
[4] C. Lin, J.A. Ritter, B.N. Popov, Characterization of sol–gel derived cobalt oxide xerogels as electrochemical capacitors, J. Electrochem. Soc. 145 (12) (1998) 4097–4103.
[5] M.R. Antono Mo Y., D.A. Scherson, In situ Ru K-edge X-ray absorption fine structure studies of electroprecipitated ruthenium dioxide film with relevance to supercapacitor applications, Phys. Chem. B 104 (9) (2000) 777.
[6] J.P. Zheng, T.R. Jow, A new charge-storage mechanism for electrochemical capacitors, J. Electrochem. Soc. 142 (1) (1995) L6–L8.
[7] J.P. Zheng, Ruthenium oxide carbon composite electrodes for electrochemical capacitors, Electrochem. Solid State Lett. 2 (8) (1999) 359–361.
[8] H.Y. Lee, J.B. Good enough, Ideal supercapacitor behavior of amorphous $V_2O_5{\cdot}nH_2O$ in potassium chloride aqueous solution, Solid State Chem. 148 (1999) 81–84.
[9] K.-C. Liu, M.A. Anderson, Porous nickel oxide/nickel film for electrochemical capacitors, J. Electrochem. Soc. 143 (1) (1996) 124–130.
[10] V. Srinivasan, J.W. Weidner, An electrochemical route for making porous nickel oxide electrochemical capacitors, J. Electrochem. Soc. 144 (8) (1997) L210–L213.
[11] http://srdata.nist.gov/xps.
[12] K.-W Nam, K.-B. Kim, J. Electrochem. Soc. 149 (3) (2002) A346.
[13] C. Natarajan, H. Matsumoto, G. Nogami, J. Electrochem. Soc. 144 (1997) 121.